

1 **Azimuthally polarized cathodoluminescence from InP nanowires**

2 B. J. M. Brenny,¹ D. van Dam,² C. I. Osorio,¹ J. Gómez Rivas,^{2,3} and A. Polman^{1, a)}

3 ¹⁾*Center for Nanophotonics, FOM Institute AMOLF, Science Park 104,*
4 *1098 XG Amsterdam, The Netherlands*

5 ²⁾*COBRA Research Institute, Eindhoven University of Technology, P.O. Box 513,*
6 *5600 MB Eindhoven, The Netherlands*

7 ³⁾*FOM Institute DIFFER, P.O. Box 6336, 5600 HH Eindhoven,*
8 *The Netherlands*

We determine the angle and polarization dependent emission from 1.75 μm and 2.50 μm long InP nanowires by using cathodoluminescence polarimetry. We excite the vertical wires using a 5 keV electron beam, and find that the 880 nm bandgap emission shows azimuthally polarized rings, with the number of rings depending on the wire height. The data agree well with a model in which spontaneous emission from the wire emitted into the far field interferes with emission reflected off the substrate. From the model, the depth range from which the emission is generated is found to be up to 400 nm below the top surface of the wires, well beyond the extent of the primary electron cloud. This enables a probe of the carrier diffusion length in the InP nanowires.

^{a)}Electronic mail: polman@amolf.nl

9 The research field of semiconductor nanowires has grown tremendously in the last
10 two decades, due to the applications in optoelectronic devices such as LEDs^{1,2}, lasers³,
11 photovoltaics^{4,5}, photodetectors⁶ and more. The electrical properties of nanowires as well as
12 their optical properties, such as the directionality and polarization of emitted radiation⁶⁻¹¹,
13 can be tuned by controlling the morphology, size, crystallinity, composition, and inclusions
14 or junctions¹²⁻¹⁶. Among the nanowire materials, indium phosphide (InP) has a bandgap
15 well-suited for photovoltaic applications, long carrier lifetime and low surface recombination
16 velocity¹⁷.

17 The light emission properties of semiconductor nanowires have mostly been studied using
18 optical excitation techniques, which are limited in spatial resolution and therefore cannot
19 access all details of the nanoscale emission mechanisms. Cathodoluminescence (CL) spec-
20 troscopy is an alternative technique that uses an electron beam as an excitation source,
21 providing high excitation resolution and accessing a broad range of material transitions and
22 defects¹⁸. Spatially-resolved CL has shown that very thin (~ 20 nm diameter) InP nanowires
23 exhibit polarized emission¹⁹. However, the angular distribution of the emitted light, which
24 is crucial for many applications, was not resolved so far.

25 In this letter, we characterize the angle- and polarization-dependent emission from InP
26 nanowires by using angle-resolved cathodoluminescence imaging polarimetry²⁰. Previous
27 studies of the directionality and polarization of semiconductor nanowires have focused
28 on wires with high-aspect-ratio dimensions, whose behavior is dominated by waveguide
29 modes^{7,10,11,21}. In contrast, here we will examine low-aspect-ratio wires. We find that the
30 angular emission from these short wires is dominated by azimuthally polarized rings that
31 are not related to waveguide modes, and demonstrate that the emission and the number
32 of rings are directly related to the wire height. The measurements are well-reproduced
33 by a point dipole scattering and interference model and provide a measure for the carrier
34 diffusion length in the wires.

35 We measured undoped InP nanowires grown vertically on an InP $\langle 100 \rangle$ substrate by a
36 combination of vapor-liquid-solid (VLS) and vapor-solid (VS) methods¹¹. Wires with an
37 initial length of $8 \mu\text{m}$ were mechanically broken, resulting in wires $1.75 \pm 0.05 \mu\text{m}$ (NW1)
38 and $2.50 \pm 0.05 \mu\text{m}$ (NW2) in length. Figures 1(a,b) show SEM images for both nanowires,
39 taken for a tilt angle of 55° . We note that both wires are tapered in shape due to the growth
40 process of the base. NW1 and NW2 are 450 and 350 nm wide at the top, respectively, and

41 are both 1.3 μm wide at the bottom of the base. This tapering will cause waveguide modes,
42 which can play a role in short wires as well²², to be ill-defined.

43 The spectra and polarization-resolved angular emission patterns of the wires were mea-
44 sured using angle-resolved cathodoluminescence imaging spectroscopy and polarimetry. The
45 emission resulting from exciting the wires with an electron beam from an SEM (5 keV, beam
46 current ~ 0.4 nA) is collected by an aluminium parabolic mirror and directed to an optical
47 setup. We can measure either the spectrum using a liquid-nitrogen-cooled back-illuminated
48 silicon CCD array (Princeton Instruments Spec-10 100B), or the angular emission profile us-
49 ing a Peltier-cooled back-illuminated 2D silicon CCD array (Princeton Instruments PIXIS
50 1024B)^{23,24}. The angular imaging mode, shown schematically in Figure 1(c), includes a
51 quarter-wave plate (QWP) and a linear polarizer (Pol.). These allow us to determine the
52 Stokes parameters and therefore the polarization of the emitted radiation, including all
53 electric field components²⁵. To achieve this we measure the intensities transmitted by six
54 different combinations of QWP and polarizer positions (horizontal, vertical, 45° , 135° , right-
55 and left-handed circular) and fully take into account the geometrical and polarization de-
56 pendent effect of the parabolic mirror on the measured emission²⁰.

57 The CL spectra of the InP nanowires peak at $\lambda_0 = 880$ nm, while the spectrum of the
58 InP substrate is centered at $\lambda_0 = 920$ nm, as we show in Figure 1(d). This blueshift in
59 the emission spectrum is due to a difference in crystal structure between the wires (mixed
60 wurtzite–zinc blende) and the substrate (zinc blende)¹¹. The spectral shape of the nanowire
61 spectrum indicates that the signal from the substrate is minimal for this measurement.
62 This is due to the relatively shallow penetration depth of the 5 keV electrons, as shown in
63 Figure 2(a), which displays the superimposed trajectories of 10^4 electrons hitting the center
64 of a 350 nm diameter InP wire, calculated using the Monte Carlo based software Casino²⁶.
65 The full interaction volume covers the entire diameter of the wire and reaches a depth of
66 ~ 250 nm, generating electron-hole pairs in this region until the electrons fully relax. The
67 large majority of excitations will take place in the first 200 nm however, as shown by the
68 dense region in Figure 2(a). The energy of the incident electrons decreases as they move
69 further into the material, reducing the energy of the carriers that can be excited.

70 The angular emission patterns of the wires exhibit a series of rings, as we show in Fig-
71 ures 3(a–d), which display the measured angular emission patterns at $\lambda_0 = 850$ nm as a
72 function of azimuthal (φ) and zenithal (θ) angles. The dark blue regions in the measure-

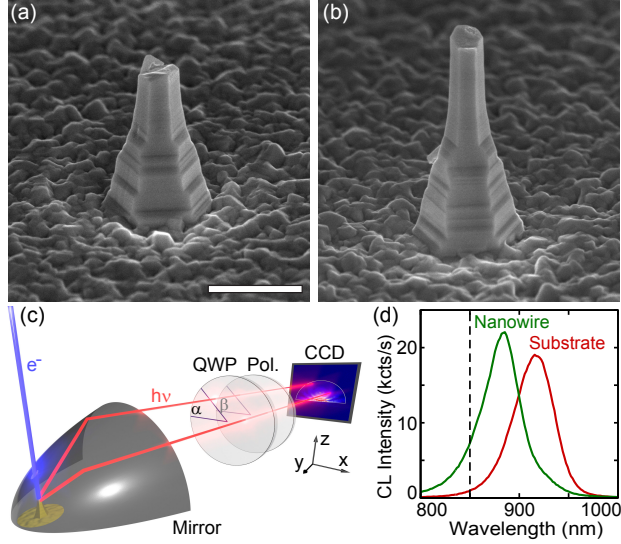


FIG. 1. Scanning electron micrographs of the InP nanowires NW1 (a) and NW2 (b), measured at a tilt angle of 55° (scale bar is $1 \mu\text{m}$ for horizontal dimensions and $1.2 \mu\text{m}$ for vertical dimensions). NW1 is $1.75 \mu\text{m}$ tall and 450 nm wide at the top; NW2 is $2.50 \mu\text{m}$ tall and 350 nm wide at the top; both wires are clearly tapered. (c) Schematic overview of the cathodoluminescence polarimetry setup. The electron beam excites the nanowires, the emitted radiation is collected by a parabolic mirror and sent through a quarter-wave plate (QWP) and linear polarizer. Bandpass filters can be used to select a certain wavelength range and the resulting beam profile is measured by the CCD camera. (d) Measured CL emission spectra of NW2 (green) and substrate (red). The spectrum of NW1 (not shown) does not differ noticeably from that of NW2. The black dashed line at $\lambda_0 = 850 \text{ nm}$ indicates the transmittance maximum of the 40 nm bandwidth bandpass filter used for the angular measurements.

73 ment correspond to the angles at which no light is collected by the mirror. Figure 3(a) shows
 74 the total intensity (I_{tot}) for NW1, while Figures 3(b,c) compare the intensity of the radially
 75 polarized field component (I_θ) to that of the azimuthally polarized field component (I_φ) for
 76 NW1. Figure 3(d) shows I_φ for NW2. These figures show that the emission is dominated
 77 by azimuthally polarized rings and that the taller NW2 exhibits more rings than NW1. The
 78 intensity trends are similar to those in previous work on the angular emission profiles of plas-
 79 monic nanoantennas, which, for a fixed wavelength, exhibit an increasing number of rings
 80 for increasing antenna height²⁷. The polarization was not resolved in this case however.

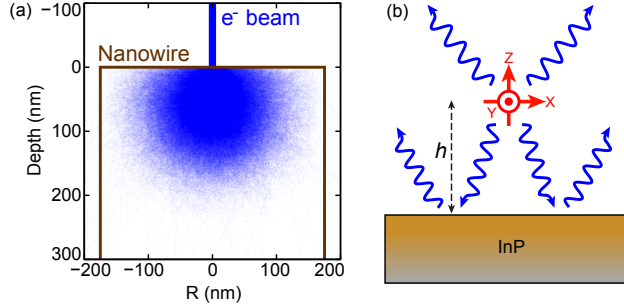


FIG. 2. (a) Monte Carlo simulation of 10^4 electrons with 5 keV energy impinging the middle of an InP nanowire, using Casino²⁶. All the electron trajectories are shown as superimposed partially transparent lines forming a blue cloud, indicating the interaction density and volume of the primary electrons with the wire. (b) Schematic of the dipole calculation. Separate X, Y and Z oriented dipoles are placed in vacuum at a height h above an InP surface. The direct emission interferes with light reflected off the substrate and the calculation produces the resulting far field radiation patterns for all field components. The field intensities for the three orthogonal dipoles are incoherently added to simulate the behavior of randomly oriented dipoles.

81 In order to analyze the emission patterns, we model the spontaneous emission of the wires
 82 as an incoherent sum of point dipoles radiating in free space above a substrate, as shown
 83 schematically in Figure 2(b). We implement the Green's function formalism and asymptotic
 84 far field approximations from Ref. 28 as they are applied in Ref. 29; the measured far field
 85 radiation results from a superposition of the emission of the dipole and its image. We
 86 calculate the far field radiation patterns for separate X, Y and Z oriented point dipoles at
 87 $\lambda_0 = 850$ nm (corresponding to the bandpass filter center wavelength) in vacuum, at a height
 88 h above an InP substrate and incoherently add the intensities for different field components.
 89 We neglect the dielectric body of the nanowire itself, placing the dipoles in vacuum, in order
 90 to keep the model simple. We find this to be a valid approach as the emission only overlaps
 91 with the nanowire body for a small portion of angular space, namely downwards where it
 92 will be guided into the substrate and absorbed. We use equal dipole amplitudes for the
 93 three orientations. The angular patterns result from the interference between the directly
 94 emitted radiation and the reflection from the substrate, and are therefore sensitive to the
 95 dipole height. The overall behavior is dominated by the X and Y dipoles, which combine to
 96 produce a strong azimuthal intensity distribution, while the Z dipole has a minor effect. To

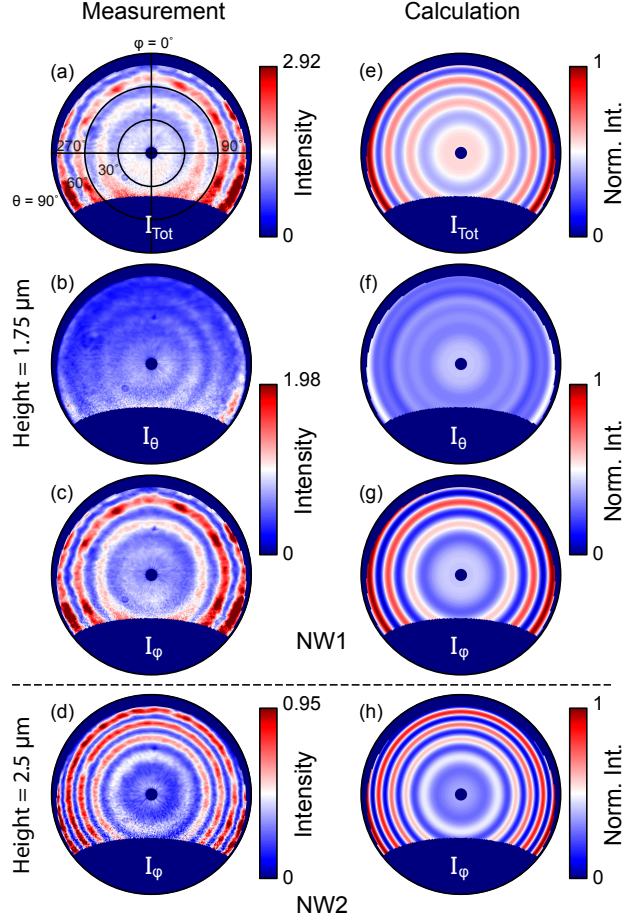


FIG. 3. Measured (a, b, c, d) and calculated (e, f, g, h) angular CL polarimetry emission intensities at $\lambda_0 = 850$ nm. The patterns were measured for central excitation of the nanowire, and the calculations averaged over a range of heights (65–415 nm below the surface, in steps of 10 nm, for both wires). (a) and (e) show the total intensity I_{tot} , (b) and (f) the radially polarized intensity I_θ , (c) and (g) the azimuthally polarized intensity I_φ , all for NW1. (d) and (h) show I_φ for NW2. The θ and φ polarized intensities for NW1 are shown on the same color scale. The calculations have been normalized to 1, while the measured intensities are given in 10^5 counts $\text{sr}^{-1} \text{s}^{-1}$.

97 reflect the electron excitation volume we have averaged the dipole positions over a range of
 98 heights, performing a calculation every 10 nm. Measurements and calculations agree best
 99 when using a height range of 350 nm, 65–415 nm below the top edge for both nanowires.
 100 The calculations accurately reproduce all major features of the measurements such as the
 101 number of rings, zenithal emission angles, relative intensities and polarization for both wires,
 102 as shown in Figures 3(e–h). We find that the averaged calculation is quite sensitive to the

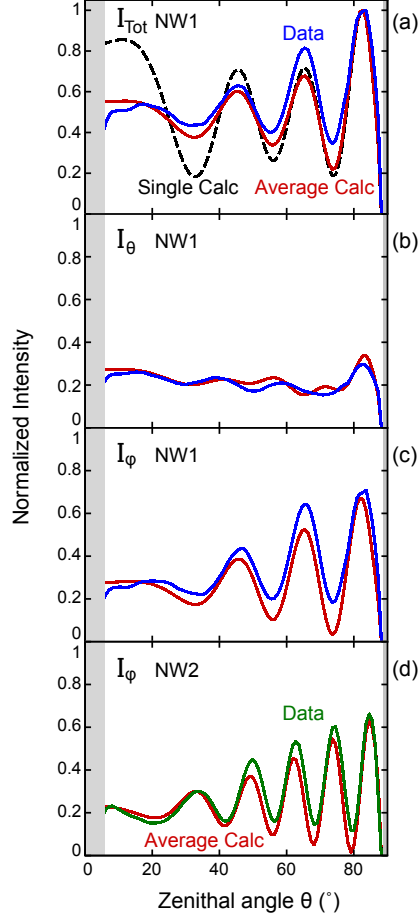


FIG. 4. Azimuthally averaged intensities from Figure 3, comparing the measurements (blue for NW1, green for NW2) to the averaged calculations (red). All measured and calculated intensities are normalized to their respective total intensity. (a), (b) and (c) show I_{tot} , I_θ and I_φ respectively for NW1, while (d) shows I_φ for NW2. In (a), the black dashed line indicates the calculation for a single height best matched to the measured data ($1.52 \mu\text{m}$). The gray areas represent the angular range not collected by the mirror.

103 chosen height range: moving the range up or down will shift the zenithal position of the rings,
 104 while increasing the range will decrease the amplitude of the intensity oscillations. A change
 105 of 10 nm or more already results in a noticeably larger difference with the measurement.

106 Examining I_{tot} for NW1 (Figures 3(a,e)), we see in both measurement and calculation a
 107 region of higher intensity in the center and three rings of increasing intensity for increasing
 108 zenithal angle. For I_θ in NW1 (Figures 3(b,f)) the features are less pronounced but we
 109 notice a thin ring at the outer edge of both measurement and calculation. Figures 3(c,g)

110 show the center disk and three rings of increasing intensity for I_φ , as for I_{tot} , confirming the
111 total emission is dominated by the azimuthally polarized contribution. We note that the
112 measured data for I_θ and I_φ are plotted with the same color scale. Finally, for I_φ in NW2
113 (Figures 3(d,h)) five rings are observed, two more than in NW1. Here too we find good
114 agreement of both zenithal emission angles and relative intensities between measurement
115 and calculation.

116 To quantitatively compare the measurements and calculations, we azimuthally average
117 the data from Figure 3 (taking into account only the angles that are collected by the mirror)
118 and show the result in Figure 4. The measured and calculated intensities are normalized
119 to their corresponding total intensity. In Figure 4(a) we also show the calculation for a
120 single dipole height for NW1 that most closely reproduces the intensity oscillations. We find
121 for a single height that the oscillations at small values of θ have a much larger amplitude
122 than in the data, while there is a very good match for the calculation that averages over
123 a height range. The height range that best fits the data for both nanowires is larger than
124 the extent of the primary electron cloud (~ 400 nm vs ~ 200 nm below the top edge of the
125 wires). It is known that carrier diffusion and photon recycling can enlarge the volume of
126 light emission³⁰. Carrier diffusion lengths of 160 nm have been measured in doped InP
127 nanowires³¹, for our undoped wires a larger diffusion length, on the order of a few hundred
128 nanometers, is expected. Rather than using a simple model in which the carrier generation
129 and light emission is fixed over a depth range, one could take into account a depth profile
130 of carrier diffusion and recombination in the wires. This will allow the CL polarimetry
131 presented here to directly determine the carrier diffusion length. Due to the high sensitivity
132 to height changes of our simple model, on the order of 10 nm, we expect that the diffusion
133 length can be resolved with a similar precision. Measurements using a range of electron beam
134 energies and thus penetration depths could be used to study the diffusion more accurately.

135 The features of I_θ in Figure 4(b) are much less pronounced than those of I_φ in Figure 4(c),
136 but in both cases there is very good agreement of the oscillations and the relative intensities,
137 which is also the case for I_φ for NW2 in Figure 4(d). A similar background signal is observed
138 for both polarizations I_θ and I_φ , indicating that the emission also contains an unpolarized
139 contribution.

140 In conclusion, we have demonstrated that InP nanowires excited by a 5 keV electron beam
141 at their top display very distinctive angular emission rings that are strongly azimuthally

142 polarized. The radiation is not dominated by the intrinsic angular emission of the nanowire
143 itself, due to the tapering and low-aspect-ratio, but by interference of the luminescence
144 with the substrate reflection. A dipolar model that calculates the interference between the
145 directly emitted light and light reflected off the substrate reproduces the measured data well.
146 The luminescence originates from a several hundred nanometer wide range near the top of
147 the wire. The depth range is the same for both wires and is larger than the primary electron
148 cloud, providing a measure for carrier diffusion in the wires. The capability to resolve
149 the spectral, angular and polarization properties of nanoscale excitation processes shows the
150 power of cathodoluminescence polarimetry as a technique to study the highly tunable optical
151 and electrical properties of semiconducting nanostructures with features much smaller than
152 the optical diffraction limit.

153 We acknowledge Femius Koenderink, Mark Knight and Toon Coenen for fruitful discus-
154 sions, and E.P.A.M. Bakkers (Eindhoven University of Technology) for providing the InP
155 sample. This work is part of the “Stichting voor Fundamenteel Onderzoek der Materie
156 (FOM)” as well as the Dutch technology foundation STW, which are financially supported
157 by the “Nederlandse Organisatie voor Wetenschappelijk Onderzoek (NWO)” and the Dutch
158 Ministry of Economic Affairs. It is also part of NanoNextNL, a nanotechnology program
159 funded by the Dutch Ministry of Economic Affairs, part of an industrial partnership pro-
160 gram between Philips and FOM, and is supported by the European Research Council (ERC).
161 A.P. is co-founder and co-owner of Delmic BV, a startup company developing a commercial
162 product based on the cathodoluminescence system that was used in this work.

163 REFERENCES

- 164 ¹K. Haraguchi, T. Katsuyama, and K. Hiruma, *J. Appl. Phys.* **75**, 4220 (1994).
165 ²C. P. T. Svensson, T. Mårtensson, J. Trägårdh, C. Larsson, M. Rask, D. Hessman,
166 L. Samuelson, and J. Ohlsson, *Nanotechnology* **19**, 305201 (2008).
167 ³M. H. Huang, S. Mao, H. Feick, H. Yan, Y. Wu, H. Kind, E. Weber, R. Russo, and
168 P. Yang, *Science* **292**, 1897 (2001).
169 ⁴J. Wallentin, N. Anttu, D. Asoli, M. Huffman, I. Åberg, M. H. Magnusson, G. Siefert,
170 P. Fuss-Kailuweit, F. Dimroth, B. Witzigmann, H. Q. Xu, L. Samuelson, K. Deppert, and
171 M. T. Borgström, *Science* **339**, 1057 (2013).

172 ⁵Y. Cui, J. Wang, S. R. Plissard, A. Cavalli, T. T. T. Vu, R. P. J. van Veldhoven, L. Gao,
173 M. Trainor, M. A. Verheijen, J. E. M. Haverkort, and E. P. A. M. Bakkers, *Nano Lett.*
174 **13**, 4113 (2013).

175 ⁶J. Wang, M. S. Gudiksen, X. Duan, Y. Cui, and C. M. Lieber, *Science* **293**, 1455 (2001).

176 ⁷A. V. Maslov and C. Z. Ning, *Opt. Lett.* **29**, 572 (2004).

177 ⁸A. Maslov, M. Bakunov, and C. Ning, *J. Appl. Phys.* **99**, 024314 (2006).

178 ⁹J. Motohisa, Y. Kohashi, and S. Maeda, *Nano Lett.* **14**, 3653 (2014).

179 ¹⁰G. Grzela, R. Paniagua-Domínguez, T. Barten, Y. Fontana, J. A. Sánchez-Gil, and
180 J. Gómez Rivas, *Nano Lett.* **12**, 5481 (2012).

181 ¹¹D. van Dam, D. R. Abujetas, R. Paniagua-Domínguez, J. A. Sánchez-Gil, E. P. A. M.
182 Bakkers, J. E. M. Haverkort, and J. Gómez Rivas, *Nano Lett.* **15**, 4557 (2015).

183 ¹²R. Yan, D. Gargas, and P. Yang, *Nat. Photonics* **3**, 569 (2009).

184 ¹³X. Duan, Y. Huang, Y. Cui, J. Wang, and C. M. Lieber, *Nature* **409**, 66 (2001).

185 ¹⁴M. S. Gudiksen, L. J. Lauhon, J. Wang, D. C. Smith, and C. M. Lieber, *Nature* **415**, 617
186 (2002).

187 ¹⁵M. Björk, B. Ohlsson, T. Sass, A. Persson, C. Thelander, M. Magnusson, K. Deppert,
188 L. Wallenberg, and L. Samuelson, *Nano Lett.* **2**, 87 (2002).

189 ¹⁶J. Claudon, J. Bleuse, N. S. Malik, M. Bazin, P. Jaffrennou, N. Gregersen, C. Sauvan,
190 P. Lalanne, and J.-M. Gérard, *Nat. Photonics* **4**, 174 (2010).

191 ¹⁷H. J. Joyce, C. J. Docherty, Q. Gao, H. H. Tan, C. Jagadish, J. Lloyd-Hughes, L. M. Herz,
192 and M. B. Johnston, *Nanotechnology* **24**, 214006 (2013).

193 ¹⁸D. Spirkoska, J. Arbiol, A. Gustafsson, S. Conesa-Boj, F. Glas, I. Zardo, M. Heigoldt,
194 M. Gass, A. Bleloch, S. Estrade, M. Kaniber, J. Rossler, F. Peiro, J. Morante, G. Abstre-
195 iter, L. Samuelson, and A. Fontcuberta i Morral, *Phys. Rev. B* **80**, 245325 (2009).

196 ¹⁹N. Yamamoto, S. Bhunia, and Y. Wantanabe, *Appl. Phys. Lett.* **88**, 153106 (2006).

197 ²⁰C. I. Osorio, T. Coenen, B. J. M. Brenny, A. Polman, and A. F. Koenderink, *ArXiv* ,
198 arXiv:1510.07976 [physics.optics] (2015).

199 ²¹J. Claudon, N. Gregersen, P. Lalanne, and J.-M. Gérard, *ChemPhysChem* **14**, 2393 (2013).

200 ²²D. J. Traviss, M. K. Schmidt, J. Aizpurua, and O. L. Muskens, *Opt. Express* **23**, 22771
201 (2015).

202 ²³T. Coenen, E. J. R. Vesseur, A. Polman, and A. F. Koenderink, *Nano Lett.* **11**, 3779
203 (2011).

- 204 ²⁴T. Coenen, E. J. R. Vesseur, and A. Polman, *Appl. Phys. Lett.* **99**, 143103 (2011).
- 205 ²⁵M. Born and E. Wolf, *Principles of Optics: Electromagnetic Theory of Propagation, In-*
206 *terference and Diffraction of Light, 7th edition* (Cambridge University Press, 1997).
- 207 ²⁶H. Demers, N. Poirier-Demers, A. R. Couture, D. Joly, M. Guilmain, N. de Jonge, and
208 D. Drouin, *Scanning* **33**, 135 (2011).
- 209 ²⁷H. Acar, T. Coenen, A. Polman, and L. Kuipers, *ACS Nano* **6**, 8226 (2012).
- 210 ²⁸L. Novotny and B. Hecht, *Principles of nano-optics* (Cambridge University press, 2006).
- 211 ²⁹F. Bernal Arango, A. Kwadrin, and A. F. Koenderink, *ACS Nano* **6**, 10156 (2012).
- 212 ³⁰N. M. Haegel, T. J. Mills, M. Talmadge, C. Scandrett, C. L. Frenzen, H. Yoon, C. M.
213 Fetzner, and R. R. King, *J. Appl. Phys.* **105**, 023711 (2009).
- 214 ³¹J. Wallentin, P. Wickert, M. Ek, A. Gustafsson, L. R. Wallenberg, M. H. Magnusson,
215 L. Samuelson, K. Deppert, and M. T. Borgström, *Appl. Phys. Lett.* **99**, 253105 (2011).